CrossMark

Novel and feasible synthetic routes to copper ferrite nanoparticles: Taguchi optimization and photocatalytic application

Sanaz Tajik[1] · Saeed Khodabakhshi[1]

Abstract In the present study, nanocrystallite copper ferrite ($CuFe_2O_4$) has been obtained via two different methods. In the first method, $CuFe_2O_4$ with an average particle size of 7.6 ± 0.5 nm was synthesized by pyrolysis of iron and cupferron as a chelating agent. In the second method, $CuFe_2O_4$ nanoparticles with an average particle size of 22.3 nm were synthesized by combined microemulsion and homogenous precipitation methods. The effective parameters for the synthesis procedures were determined and optimized using L_8 and L_4 Taguchi designs. Different techniques to characterize the structure and morphological properties of nanoparticles are X-ray diffraction, thermogravimetric analysis, scanning electron microscopy, Brunauer–Emmett–Teller, transmission electron microscopy, Dynamic light scattering, and elemental micro analysis. Crystal violet ($C_{25}N_3H_{30}Cl$) as a model pollutant and UV lamp as an energy source were applied for the investigation of the photocatalytic activity of nanocrystalline $CuFe_2O_4$ powders. The 97 % degradation of crystal violet could be obtained around 100 min.

1 Introduction

Copper ferrite is well-known as the most technologically useful spinel ferrite [1] because of a wide range of applications. For example, it is used as a gas sensing material [2], an active catalyst in organic reactions [3, 4], and high density magnetic recordings. Besides, copper ferrite has been employed in ferrofluid technology, microwave devices, and data storage [5–10]. Nanosized copper spinel ferrite shows unusual properties in comparison with its bulk analog and has received great attention during last decade.

So far, various methods such as solid state reaction [11], mechanochemical [12], sol–gel [13], co-precipitation [14], combustion synthesis [15], complexation methods [16, 17], microemulsion [18, 19] and hydro/salvo thermal synthesis [20, 21] have been reported to synthesize copper ferrite. In all technological applications of copper ferrite, some properties such as high specific surface area (SSA), high purity, and low average particle size with narrow size range are of prime importance. In this study, we report two novel methods for the preparation of porous and high purity $CuFe_2O_4$ nanocrystallites. In the first, a stoichiometric mixture of mixed copper (II) and iron (III) cupferron chelates were thermalized to obtain a high porosity product. The second method is the combination of microemulsion and proposed complete homogeneous precipitation in which all reactants are homogeneously generated. In the proposed procedure, the Cu^{2+} and Fe^{3+} cations were generated from $K_2Cu(CN)_4$ and $K_3Fe(CN)_6$ by unmasking reactions and the precipitating agent (NaOH) was generated simultaneously by hydrolysis of sodium acetate. The advantages of homogeneous precipitation are high purity and crystallinity of the product [22].

Taguchi statistical design was also employed for the process optimization and investigation of the most effective factors on the particle size of the products [23]. Although the precipitation method has been widely employed to synthesize fine nanostructures [24–26], the chelate thermolysis and combined homogenous precipitation and microemulsion methods proposed in the present study were not found in the open literature.

✉ Saeed Khodabakhshi
saeidkhm@yahoo.com

[1] Department of Chemistry, Robatkarim Branch, Islamic Azad University, Robatkarim, Iran
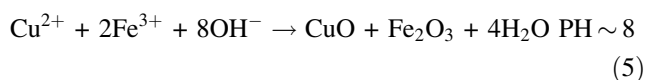
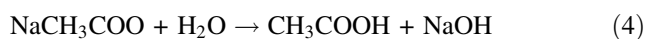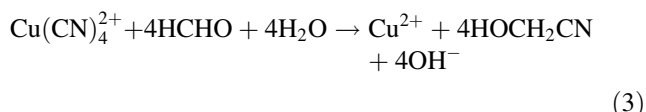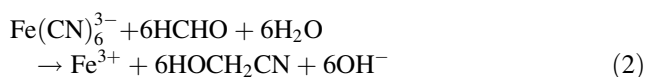🍨 Springer

2 Results and discussion

The chelating agent cupferron (Cpf) is the ammonium salt of N-nitroso-N-phenyl hydroxylamine. The chemical formula of Cpf and its Cu (II) and Fe (III) chelates are given in Fig. 1.

The Cpf is a bidentate chelating agent in which the anion reacts with Cu (II) and Fe (III) metal ions through its nitrogen and oxygen atoms. The resulting four membered ring chelates are stable and insoluble in aqueous solutions. The formation of metal chelates was confirmed by elemental micro analysis of products (Table 1). The equation for the thermolysis of the mixed chelate is:

$$Cu\ (C_6H_5N_2O_2)_2 + 2\ Fe\ (C_6H_5N_2O_2)_3 + 104/2\ O_2$$
$$\rightarrow CuFe_2O_4 + 20H_2O + 48CO_2 + 8N_2 \tag{1}$$
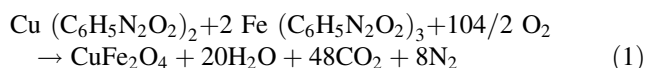
The exit of high amounts of hot gases from the bulk chelates during thermolysis causes a loss of heat from the solid phase and favors the porosity and formation of small particles.

The chemical reactions of the second procedure for the formation of $CuFe_2O_4$ are:

$$Fe(CN)_6^{3-} + 6HCHO + 6H_2O$$
$$\rightarrow Fe^{3+} + 6HOCH_2CN + 6OH^- \tag{2}$$

$$Cu(CN)_4^{2+} + 4HCHO + 4H_2O \rightarrow Cu^{2+} + 4HOCH_2CN$$
$$+ 4OH^- \tag{3}$$

$$NaCH_3COO + H_2O \rightarrow CH_3COOH + NaOH \tag{4}$$

$$Cu^{2+} + 2Fe^{3+} + 8OH^- \rightarrow CuO + Fe_2O_3 + 4H_2O\ PH \sim 8 \tag{5}$$

$$CuO + Fe_2O_3 \rightarrow CuFe_2O_4 \tag{6}$$

2.1 Thermogravimetric analysis (TGA)

Figure 2 shows the thermogravimetric (TG) curve of the dried mixed chelates. According to the curve, the first weight loss step at 100–150 °C is attributed to the loss of physisorbed and interlayer water. The major weight loss in the range of 150–250 °C is due to decomposition of the chelate complex and combustion of organic species. There is no weight loss around 550–830 °C. The weight of residue is in agreement with $CuFe_2O_4$ (94 %).
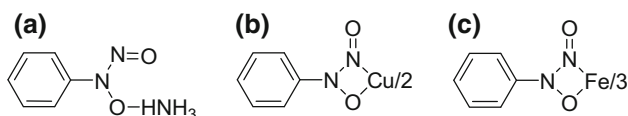

Fig. 1 a Cpf, b Cu (Cpf)$_2$, c Fe (Cpf)$_3$

2.2 FT-IR analysis

As a representative sample, the Fig. 3 shows the FT-IR spectrum for the nano-$CuFe_2O_4$ synthesized by mixed cupferron chelates thermolysis. Two characteristic bands in the range of 400–600 cm^{-1} correspond to the stretching vibration of Fe^{3+}–O^{2-} and Cu^{2+}–O^{2-} [27].

Table 1 Elemental analysis of copper (II) and iron (III) complexes

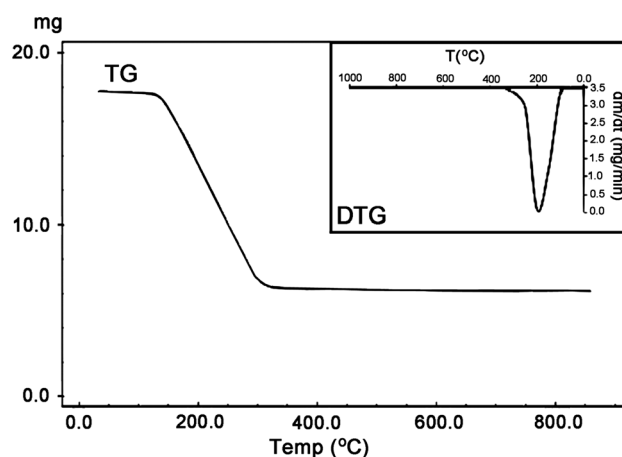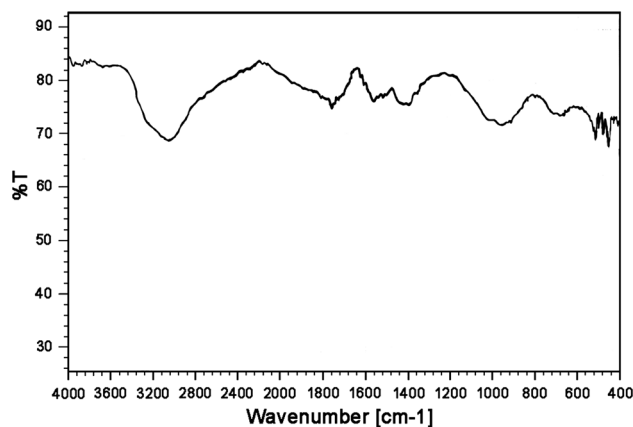|	% Elements		
	C	H	N
Cu(C$_6$H$_5$N$_2$O$_2$)$_2$ required	42.7	2.9	16.6
Found	42.8	2.8	16.5
Fe(C$_6$H$_5$N$_2$O$_2$)$_3$ required	46.3	3.2	17.9
Found	46.4	3.0	18.0

Fig. 2 TG curve for nano-$CuFe_2O_4$

Fig. 3 FT-IR spectrum for $CuFe_2O_4$ nanoparticles

2.3 Powder X-ray diffraction (XRD)

The XRD patterns of $CuFe_2O_4$ samples prepared by the proposed methods are given in Fig. 4a, b.

All of the diffraction peaks can be indexed to the tetragonal phase structured $CuFe_2O_4$ with lattice constants of a = 5.8444 and c = 8.6304 Å which are in good agreement with the standard data from JCPDS Card No. 00-034-0425. Scherer's formula $(L = k\lambda/\beta\cos\theta)$ was applied to obtain the crystallite sizes of the $CuFe_2O_4$ spinel powders. Where λ is the wavelength of the radiation (0.15406 nm), θ is the Bragg angle, K is a constant (0.9), and L is the average crystallite size. The half-width of the diffraction line (in radians) was taken as the experimental half-width (β_{exp}) and corrected for the experimental broadening (β_{instr}) according to Eq. (7):

$$\beta(2\theta) = \left(\beta_{exp}^2 - \beta_{instr}^2\right)^{(1/2)} \tag{7}$$

β_{instr} was experimentally measured using silicon powder. The average crystal diameters obtained were selected as responses of the experiments and are shown in Table 2. According to the Table, it can be concluded that all samples were nanocrystalline copper ferrite and the average crystalline size for chelate thermolysis and microemulsion procedures varied between 8.20 and 13.20 nm and 22.30 and 29.40 nm, respectively. The smaller particle sizes belong to the conditions of row 5 of Table 5 and row 4 of Table 6 for procedures 1 and 2, respectively.

The factor mean effect (E_f) was calculated to determine which factor has the most effect on the response value by the use of the following equation [28].

Table 2 Average crystallite size of samples

Sample	Average crystal size (nm)	
	Chelate thermolysis	Microemulsion
1	y_1 = 10.40	y_1 = 29.40
2	y_2 = 11.90	y_2 = 27.20
3	y_3 = 8.60	y_3 = 25.00
4	y_4 = 9.70	y_4 = 22.30
5	y_5 = 8.20	
6	y_6 = 9.00	
7	y_7 = 13.20	
8	y_8 = 11.20	

Factor Mean Effect

$$= \left[\frac{\sum_{i=1}^{r}(Results\ of\ high\ level)_i - \sum_{i=1}^{r}(Results\ of\ low\ level)_i}{r/2} \right] \tag{8}$$

where r is the number of runs

The results of E_f for the chelate thermolysis method are shown in Table 3. Results of calculation show that the factors C (stirring rate) and E (calcination temperature) have the main effects on the average crystal size. Other factors A, B, D, F, and G do not show a greater effect on the average crystal size. To check these results, the main effect plot of factors was obtained by minitab software (Fig. 5). The higher slopes of the lines indicate the bigger

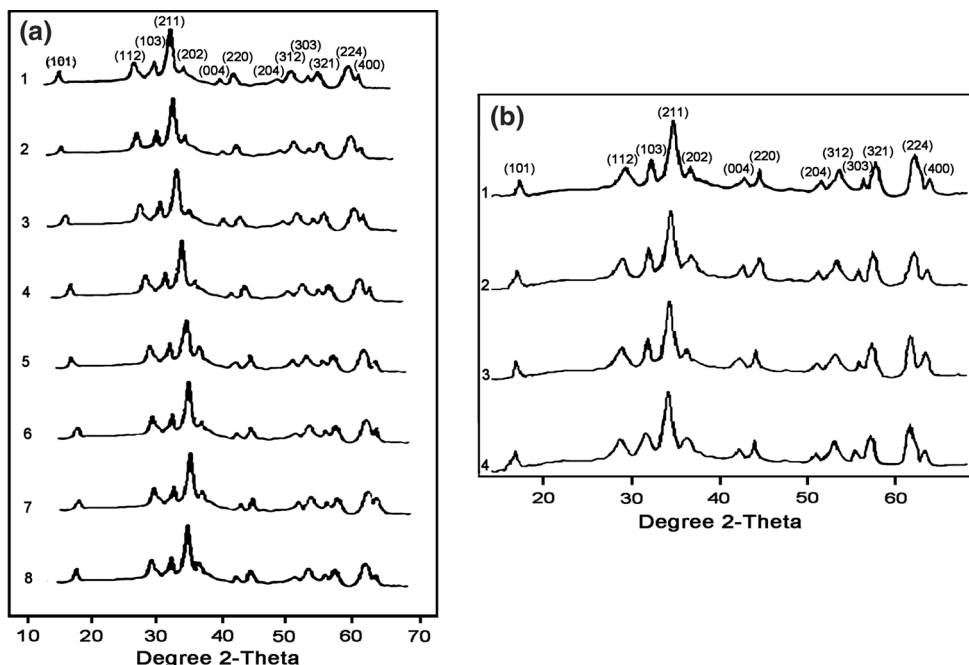**Fig. 4** X-ray powder diffraction pattern of $CuFe_2O_4$ obtained by **a** thermolysis procedure and **b** microemulsion procedure

Table 3 The E_f data for factors (chelate thermolysis method)

Level	Factor						
	A	B	C	D	E	F	G
1	10.15	9.88	11.68	10.10	9.80	9.88	10.58
2	10.40	10.68	8.88	10.45	10.75	10.68	9.98
E_f	0.25	0.80	2.80	0.35	0.95	0.80	0.60

Table 4 The E_f data for factors (microemulsion-homogeneous method)

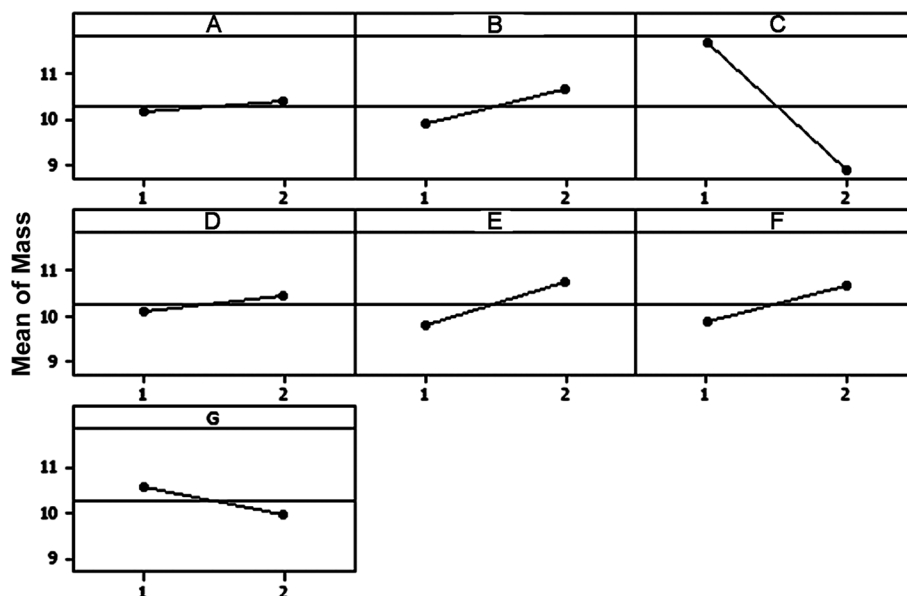| Level	Factor		
	A	B	C
1	28.30	27.20	25.85
2	23.65	24.75	26.10
E_f	4.65	2.45	0.25

effect of the corresponding factor. The results are comparable with the calculated E_f.

The prediction of the optimized crystallite size is obtained from the following formula:

$$T = \frac{\sum_{i=1}^{8} L_i}{8} = 10.27 \tag{9}$$

$$\begin{aligned} Y_{opt} = {} & T + (A_x - T) + (B_x - T) + (C_x - T) + (D_x - T) \\ & + (E_x - T) + (F_x - T) + (G_x - T) \\ = {} & 7.05 \end{aligned} \tag{10}$$

In Eq. (9), T is the grand average of the responses and in Eq. (10) Y_{opt} is the predicted crystal size under optimum conditions. To confirm the accuracy of the obtained results, a sample was prepared under optimum conditions (A = 1, B = 1, C = 2, D = 1, E = 1, F = 1, and G = 2) and named sample 9. The crystal size of sample 9 was measured by Scherer's formula to be 7.60 nm. The difference between the predicted (7.05 nm) and achieved values (7.60 nm) and 8.20 nm which is the response value of sample 5 (Table 2) is negligible and confirms the good predictability of the process and accuracy of the experimental results.

In the microemulsion-homogeneous procedure as indicated in Table 4, E_f for type of organic phase (A) was higher than others, so it is the more significant factor in synthesizing copper ferrite nanoparticles. The main effect plots of factors (Fig. 6) confirm that A = 2, B = 2, and C = 1 can be considered as the optimum condition to reach minimum response.

The prediction of the optimized crystallite size was calculated from the following formula:

$$T = \frac{\sum_{i=1}^{4} L_i}{4} = 25.98 \tag{11}$$

$$Y_{opt} = T + (A_x - T) + (B_x - T) + (C_x - T) = 22.30 \tag{12}$$

The calculated value is the same as the response of row 4 of L_4 Taguchi array for the microemulsion method (Table 2) confirming the accuracy of the method.

2.4 Brunauer–Emmett–Teller (BET)

The specific surface area (SSA) of the optimized $CuFe_2O_4$ sample synthesized by thermolysis procedure was calculated according to the BET method by using the data of adsorption of nitrogen on the sample at 77°K.

Fig. 5 The main factor effect plot in mixed chelates thermolysis approach

Fig. 6 The main factor effect plot in microemulsion-homogeneous approach
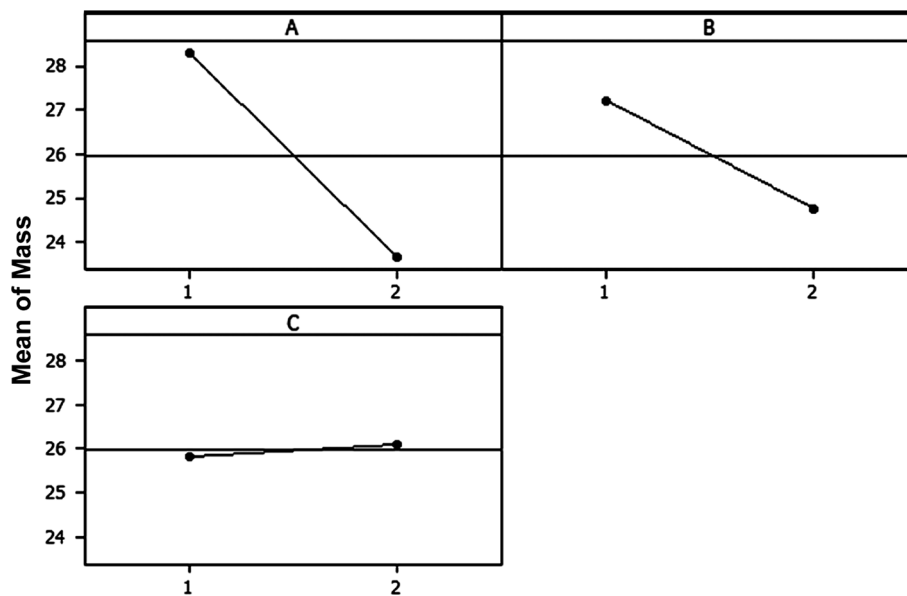
On the basis of the calculation, the SSA of the sample was determined as 144.4 m^2/g which is higher than the maximum of the reported value in the literature [29]. Equation (13) was used to estimate the SSA of the spherical particles.

$$D = \frac{6}{S_{sp}d_s} \tag{13}$$

where d_s is the density of the solid, S_{sp} is the specific surface area, and D is the average particle size. d_s for $CuFe_2O_4$ is 5.40 (g/cm^3) and also D for the optimized conditions is 7.60 nm, therefore, the calculated S_{sp} of the powder is 146.2 m^2/g which meets the experimental results.

2.5 Scanning electron microscopy (SEM)

SEM images of the $CuFe_2O_4$ nanoparticles synthesized according to the optimum conditions are shown in Fig. 7. As can be seen, the nanoparticles in methods 1 and 2 are relatively spherical with the diameter of 4.0–12.0 and 11.0–33.0 nm, respectively.

2.6 Dynamic light scattering (DLS) and transmission electron microscopy (TEM)

The DLS size distribution curves and the TEM images for the optimized samples obtained according to the optimized condition for procedures 1 and 2 are presented in Figs. 8 and 9, respectively.

It should be noted that the samples were dispersed in water by sonication before these studies. The data obtained are in agreement with the previous results.

2.7 Photocatalytic activity of $CuFe_2O_4$

Photocatalytic activity of copper ferrite particles was evaluated by measuring the photocatalytic degradation of crystal violet (CV) in water under the illumination of UV light. The initial concentration of CV was 1 ppm with λ_{max}
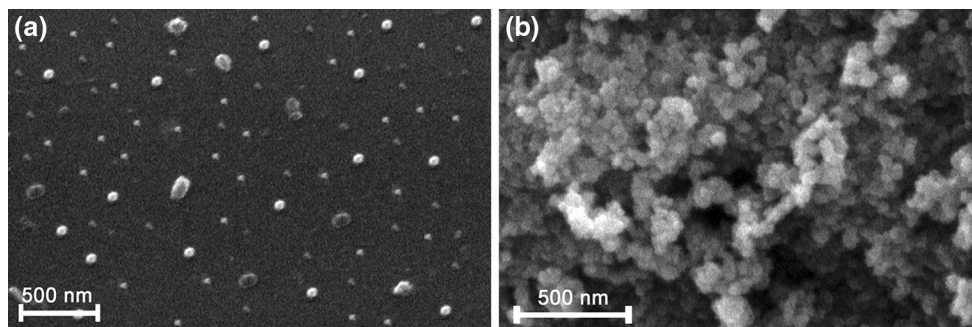

Fig. 7 SEM images of $CuFe_2O_4$ nanoparticles via **a** thermolysis procedure and **b** microemulsion procedure
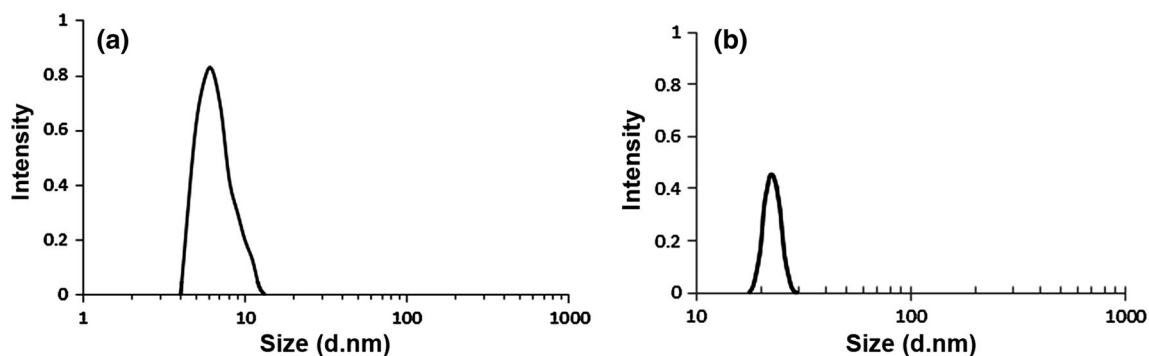
Fig. 8 Particle size ranges obtained by DLLS **a** procedure 1, mean diameter 7.7 nm and particle size range 4.2–13.5 nm **b** procedure 2, mean diameter 22.5 nm and particle size range 18–28 nm
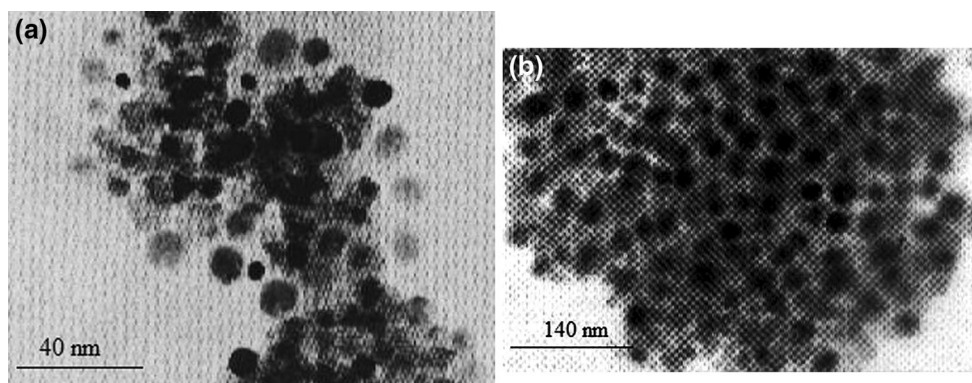

Fig. 9 TEM images of $CuFe_2O_4$ **a** procedure 1 (4.5–12.3 nm) **b** procedure 2 (17.6–29.0 nm)

in 575 nm ($\varepsilon = 5 \times 10^4\ M^{-1}\ cm^{-1}$). The $CuFe_2O_4$ nanoparticles (0.009 g) synthesized according to optimum conditions by chelate thermolysis were added to 50 mL CV and sample 2 was taken as a blank with no $CuFe_2O_4$. Figure 10 shows the results of the photocatalytic degradation of CV by $CuFe_2O_4$. According to the diagram, there

was no change in CV concentration for sample 2 after 100 min of illumination, meaning that there was no degradation in CV without $CuFe_2O_4$ under radiation. However in the presence of $CuFe_2O_4$, 97 % degradation could be achieved at 100 min after illumination.
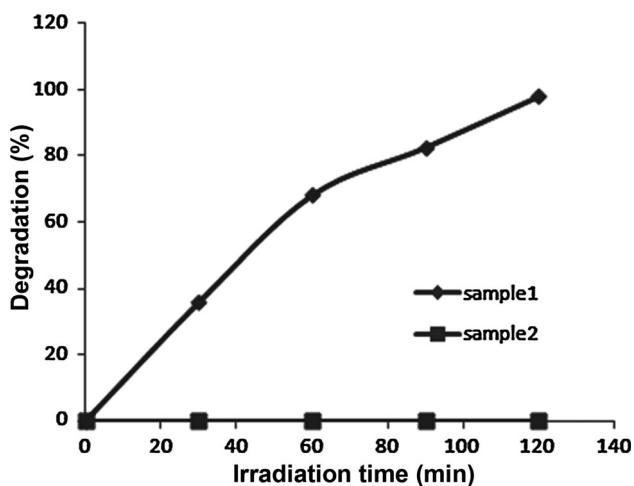
3 Conclusion

The nanoparticles of $CuFe_2O_4$ were synthesized by two novel methods using thermolysis of mixed cupferron chelates and improved microemulsion. Nanoparticles were analyzed and characterized by XRD, TGA, BET, SEM, TEM, DLS, and chemical analysis. The optimum responses for the preparing smaller nanocrystallites were obtained by L_8 and L_4 Taguchi experimental designs. The nano copper ferrite (average particle size of 7.6 ± 0.5 nm, SSA = 144.4 m²/g and the overall yield of 99.8 %) was prepared by mixed cupferron thermolysis of copper (II) and iron (III) chelates. The product obtained by the combined microemulsion and homogeneous precipitation method had high purity (average particle size of 22.3 nm and yield of 97 %). The good quality and very high yield of nano

Fig. 10 Diagram of degradation of crystal violet

$CuFe_2O_4$ obtained by mixed chelates thermolysis makes it suitable for industrial applications.

4 Experimental

4.1 Materials

All chemicals were purchased from Merck. Distilled deionized water was used in all experiments.

4.2 Characterization

Powder X-ray diffraction measurements were made on a Philips X'pert diffractometer, using filtered $Cuk\alpha$ radiation. Thermogravimetric analysis measurement was performed on a Shimadzu TG50 analyzer. A Philips XL30 instrument used to record SEM micrographs. Specific surface area (SSA) of $CuFe_2O_4$ was measured based on the principle of N_2 sorption with Brunauer–Emmet–Teller (BET) surface analyzer (SA 3100. Coulter, USA). Dynamic Light Scattering (DLS) analysis was carried out with SEMATECH Wyatt QELS (230 V, 50 Hz). The CHN-micro, Karl Kolb 267-48 was used for elemental analysis. Ultraviolet–visible (UV–Vis) spectroscopy was carried out using Cintra5, GBC Scientific spectrophotometer equipment. The images of $CuAl_2O_4$ nanocrystals were obtained with JEDL-JFM-1200 EX transmission electron microscopy (TEM).

4.3 Synthesis by mixed cupferron chelates thermolysis (procedure 1)

All samples were prepared according to a combination of factors and levels shown in Table 5 (Taguchi L_8 statistical design which is discussed later).

In a typical experiment, appropriate stoichiometric amounts of copper and iron salts were dissolved in water and stirred well. After that the aqueous solution of the complexing agent (Cpf) was added to the solution to form

Table 5 Taguchi L_8 statistical design array

Experiment no	Randomized order	Factors						
		A	B	C	D	E	F	G
1	2	1	1	1	1	1	1	1
2	6	1	1	1	2	2	2	2
3	1	1	2	2	1	1	2	2
4	8	1	2	2	2	2	1	1
5	3	2	1	2	1	2	1	2
6	7	2	1	2	2	1	2	1
7	4	2	2	1	1	2	2	1
8	5	2	2	1	2	1	1	2

mixed chelates. The brown product was filtered through a sintered glass crucible and washed with distilled water several times to remove any residual impurity. Subsequently, the product was dried in an air oven for 2 h at 100 °C followed by calcination at 700 °C for 2 h to obtain $CuFe_2O_4$, whit a 99.8 % yield.

4.4 Synthesis by microemulsion method (procedure 2)

All samples were prepared according to a combination of factors and levels shown in Table 6.

In a typical experiment, two microemulsions (I and II) were prepared containing appropriate stoichiometric amounts of initial materials. The amount of aqueous phase and organic phase are the same as Ref. [30] and are indicated in Table 7. The prepared microemulsions were mixed together and left for 3 h at room temperature. The pH of the solution was about 8. Finally, the obtained precipitate was separated by centrifugation and washed thoroughly with absolute ethanol and hot water several times to remove impurities. Afterward, the product was dried at 120 °C in an air oven and calcinated at 700 °C for 2 h to produce nano $CuFe_2O_4$ (yield 97 %).

4.5 Experimental design

Taguchi L_8 and L_4 orthogonal array, as shown in Tables 5 and 6, were used for investigating the effective factors in the synthesis of copper ferrite powders by thermolysis of mixed cupferron chelates and the microemulsion method,

Table 6 Taguchi L_4 statistical design array

Experiment no	Randomized order	Factors		
		A	B	C
1	2	1	1	1
2	3	1	2	2
3	1	2	1	2
4	4	2	2	1

Table 7 The amount of aqueous and organic phases in microemulsion I and II

	I	II	V(ml)
Aqueous phase	$K_2Cu(CN)_4$, $K_3Fe(CN)_6$	HCHO, $NaCH_3COO$	10
Surfactant	CTAB	CTAB	10
Co-surfactant	Cyclohexanol	Cyclohexanol	10
Oil phase	n-Hexane	n-Hexane	70

Table 8 Factors and their levels in thermolysis of cupferron chelate method (procedure 1)

Factors	Levels	
	1 Nitrate	2 Sulfate
A. Type of metal salts		
B. Concentration ratio of Cpf:precursors	1:1	2:1
C. Stirring rate (rpm)	500	700
D. Molarities of Cpf	0.01	0.02
E. Calcinations temperature (°C)	600	700
F. Concentration of metal precursors	0.01, 0.02	0.02, 0.04
G. Calcinations time (min)	120	180

Table 9 Factors and their levels in microemulsion method (procedure 2)

Factor	Level	
	1	2
A. Organic phase, co-surfactant	n-Hexane, cyclohexanol	Octanol
B. Stirring rate (rpm)	900	1200
C. Initial of metal concentration precursors (M)	0.05, 0.1	0.1, 0.2

respectively. The factors and their levels considered are shown in Tables 8 and 9.

References

1. G.F. Goyz, H.R. Rechenberg, Nanostruct. Mater. **10**, 1001 (1998)
2. Z. Sun, L. Lin, D. Zengjia, W. Pan, Sensor Actuat. B-Chem. **125**, 144 (2007)
3. N.M. Deraz, Anal. J. Appl. Pyrolysis **82**, 212 (2008)
4. M.H. Khedr, A.A. Farghali, A.A. Abdel-Khalek, J. Anal. Appl. Pyrolysis **78**, 1 (2007)
5. S. Sun, C.B. Murrey, B. Weller, L. Folks, B. Morse, Science **287**, 1989 (2000)
6. C. Liu, B.S. Zou, A.J. Rondinone, Z.J. Zhang, J. Phys. Chem. B **104**, 1141 (2000)
7. A. Cabanas, M. Poliakoff, J. Mater. Chem. **11**, 1408 (2001)
8. J. Du, Z. Liu, W. Wu, Z. Li, B. Han, Y. Huang, Mater. Res. Bull. **40**, 928 (2005)
9. J.Z. Jiang, G.F. Goya, H.R. Rechenberg, J. Phys. Condens. Mater. **11**, 4063 (1999)
10. P.B. Pandyo, H.H. Joshi, R.G. Kulkarni, J. Mater. Sci. **10**, 474 (1991)
11. J.E. Tasca, C.E. Quincoces, A. Lavat, A.M. Alvarez, M.G. Gonzglez, Ceram. Int. **37**, 803 (2011)
12. E. Manova, T. Tsoncheva, D. Paneva, M. Popova, N. Velinov, B. Kunev, K. Tenchev, I. Mitov. J. Solid State Chem. **184**, 1153 (2011)
13. S. Bassaid, M. Chaib, S. Omeiri, A. Bouguelia, M. Trari, J. Photochem. Photobiol. **201**, 62 (2009)
14. S.S. Yattinahalli, S.B. Kapatkar, N.H. Ayachit, S.N. Mathad, Int. J. Self-Propag. High-Temp. Synth. **22**, 147 (2013)
15. T. Liu, L. Wang, P. Yang, B. Hu, Mater. Lett. **62**, 4056 (2008)
16. S. Yan, J. Geng, L. Yin, E. Zhou, J. Mogn. Mater. **277**, 84 (2004)
17. G. Marinescu, L. Patron, O. Carp, L. Diamandescu, N. Staricu, S. Meghea, M. Buezeanu, J.C. Grenier, J. Etourneau, J. Mater. Chem. **12**, 3458 (2002)
18. A. Kosak, D. Makovec, A. Zenidarzic, M. Dropenik, J. Eur. Ceram. Soc. **24**, 959 (2004)
19. C. Liu, Z.J. Zhang, Chem. Mater. **13**, 2092 (2001)
20. J. Wang, F. Ren, R. Yi, A. Yan, G. Qiu, X. Liu, J. Alloy. Compd. **479**, 791 (2009)
21. S. Verma, P.A. Joy, Y.B. Khollam, H.S. Potdor, S.B. Despande, Mater. Lett. **58**, 1092 (2004)
22. E.C. Sousa, C.R. Alves, R. Aguino, M.H. Sousa, G.F. Gya, H.R. Recherberg, F.A. Torinho, J. Depeyrot, J. Magn. Magn. Mater. **289**, 118 (2005)
23. R.K. Roy, *Design of Experiments Using Taguchi Approach* (Wiley, New York, 2001)
24. M. Ramezani, S.M. Hosseinpour-Mashkani, A. Sobhani-Nasab, H. Ghasemi Estarki, J. Mater. Sci. Mater. Electron **26**, 7588 (2015)
25. S. Mostafa Hosseinpour-Mashkani, M. Ramezani, A. Sobhani-Nasab, M. Esmaeili-Zare, J. Mater. Sci. Mater. Electron **26**, 6086 (2015)
26. A. Gholami, M. Maddahfar, J. Mater. Sci. Mater. Electron. **26**, 7745 (2015)
27. K. Pradhan, S. Paul, A.R. Das, Catal. Sci. Technol. **4**, 822 (2014)
28. L. Jun, M. Junfeng, L. Botao, Ceram. Int. **34**, 1557 (2008)
29. A. Douglas, M.S. Donald, F.J. Holler, *Fundamentals of Analytical Chemistry*, 5th edn. (Sunders, Philadelphia, 1996)
30. M.M. Rashad, R.M. Mohamed, M.A. Ibrahim, L.F.M. Ismail, E.A. Abdel-Aal, Adv. Powder Technol. **23**, 315 (2012)